



## Short communication

## A cheap asymmetric supercapacitor with high energy at high power: Activated carbon//K<sub>0.27</sub>MnO<sub>2</sub>·0.6H<sub>2</sub>O

Qunting Qu<sup>a</sup>, Lei Li<sup>a</sup>, Shu Tian<sup>a</sup>, Wenling Guo<sup>a</sup>, Yuping Wu<sup>a,\*,</sup>, Rudolf Holze<sup>b,\*</sup>

<sup>a</sup> New Energy and Materials Laboratory (NEML), Department of Chemistry, Shanghai Key Laboratory of Molecular Catalysis and Innovative Materials, Fudan University, Shanghai 200433, China

<sup>b</sup> Technische Universität Chemnitz, Institut für Chemie, D-09107 Chemnitz, Germany

## ARTICLE INFO

## Article history:

Received 4 August 2009

Received in revised form 9 September 2009

Accepted 20 October 2009

Available online 13 November 2009

## Keywords:

Supercapacitor

K<sub>0.27</sub>MnO<sub>2</sub>

K<sup>+</sup>

Electrochemical behavior

Aqueous electrolyte

## ABSTRACT

Studies of the electrochemical behavior of K<sub>0.27</sub>MnO<sub>2</sub>·0.6H<sub>2</sub>O in K<sub>2</sub>SO<sub>4</sub> show the reversible intercalation/deintercalation of K<sup>+</sup>-ions in the lattice. An asymmetric supercapacitor activated carbon (AC)/0.5 mol l<sup>-1</sup> K<sub>2</sub>SO<sub>4</sub>/K<sub>0.27</sub>MnO<sub>2</sub>·0.6H<sub>2</sub>O was assembled and tested successfully. It shows an energy density of 25.3 Wh kg<sup>-1</sup> at a power density of 140 W kg<sup>-1</sup>; at the same time it keeps a very good rate behavior with an energy density of 17.6 Wh kg<sup>-1</sup> at a power density of 2 kW kg<sup>-1</sup> based on the total mass of the active electrode materials, which is higher than that of AC/0.5 mol l<sup>-1</sup> Li<sub>2</sub>SO<sub>4</sub>/LiMn<sub>2</sub>O<sub>4</sub>. In addition, this asymmetric supercapacitor shows excellent cycling behavior without the need to remove oxygen from the electrolyte solution. This can be ascribed in part to the stability of the lamellar structure of K<sub>0.27</sub>MnO<sub>2</sub>·0.6H<sub>2</sub>O. This asymmetric aqueous capacitor has great promise for practical applications due to high energy density at high power density.

© 2009 Elsevier B.V. All rights reserved.

## 1. Introduction

Supercapacitors or electrochemical double layer capacitors (EDLCs) have promising applications as backup or auxiliary power sources in electric vehicles or other electronic devices for the purpose of power enhancement since their power density is very high (2–5 kW kg<sup>-1</sup>). However, the substitution of supercapacitors for current batteries remains to be a challenge owing to their very low energy density (<10 Wh kg<sup>-1</sup>).

Recently, hybrid systems were explored by utilizing the high energy density of batteries, especially lithium ion batteries, in combination with high power density of supercapacitors [1–11]. A case in point is the hybrid system activated carbon (AC)//LiMn<sub>2</sub>O<sub>4</sub>, which utilizes the lithium ion intercalation compound LiMn<sub>2</sub>O<sub>4</sub> as cathode, activated carbon as anode and 1 mol l<sup>-1</sup> Li<sub>2</sub>SO<sub>4</sub> as electrolyte [3]. However, owing to the three-dimensional tunnel structure of spinel-type LiMn<sub>2</sub>O<sub>4</sub>, the ionic diffusion during the charge-discharge is more restricted than in the two-dimensional lamellar structure. In addition, the hydrated radius of Li<sup>+</sup> is larger and thus its conductivity is lower than those of Na<sup>+</sup> and K<sup>+</sup>. As a result, the energy density of AC//LiMn<sub>2</sub>O<sub>4</sub> is low at high power,

which limits its practical application. Moreover, the theoretical capacity of spinel LiMn<sub>2</sub>O<sub>4</sub> is not sufficiently high since the intercalation amounts of Li<sup>+</sup> ions into spinel Li<sub>x</sub>Mn<sub>2</sub>O<sub>4</sub> are limited to the range of 0 ≤ x ≤ 1, i.e., the maximum value of Li/Mn ratio is 0.5. Therefore, LiMnO<sub>2</sub> with a two-dimensional lamellar structure and a Li/Mn ratio of 1.0 is expected to exhibit better rate capability and higher theoretical capacity than its spinel form. However, the lamellar structure of LiMnO<sub>2</sub> has been demonstrated to be unstable during cycling and it transforms into the spinel form easily since the lamellar compound has a cubic-close-packed arrangement of oxide ions which is identical to that of a spinel [12–14].

Introduction of large alkali ions and H<sub>2</sub>O molecules into the interlayer space of manganese oxide could stabilize the lamellar structure [15,16]. For example, lamellar K<sub>x</sub>MnO<sub>2</sub>, with the large K<sup>+</sup> ions as pillars, shows better cycling performance than Li<sub>x</sub>MnO<sub>2</sub> during the Li<sup>+</sup> intercalation/deintercalation in organic electrolytes. This can be ascribed to the expansion of the interlayer space. At the same time, large K<sup>+</sup> ions make manganese cations diffusion into the interlayer region to form spinel structure less favorable [14]. Introduction of H<sub>2</sub>O into the interlayer space of MnO<sub>2</sub> also plays an important role in the stability of lamellar MnO<sub>2</sub> [17]. When K<sub>x</sub>MnO<sub>2</sub>·yH<sub>2</sub>O is used as electrode material in an aqueous capacitor, the existence of these interlayer H<sub>2</sub>O molecules is not supposed to influence the performance of the capacitor, unlike commercial lithium-ion batteries using organic electrolytes, which require anhydrous environment for the assembly of battery. In addition, lamellar K<sub>x</sub>MnO<sub>2</sub>·yH<sub>2</sub>O lattice possesses a large inter-

\* Corresponding author. Tel.: +49 37153131509; fax: +49 37153121269.

\*\* Corresponding author. Tel.: +86 21 55664223; fax: +86 21 55664223.

E-mail addresses: [wuyp@fudan.edu.cn](mailto:wuyp@fudan.edu.cn) (Y. Wu), [rudolf.holze@chemie.tu-chemnitz.de](mailto:rudolf.holze@chemie.tu-chemnitz.de) (R. Holze).

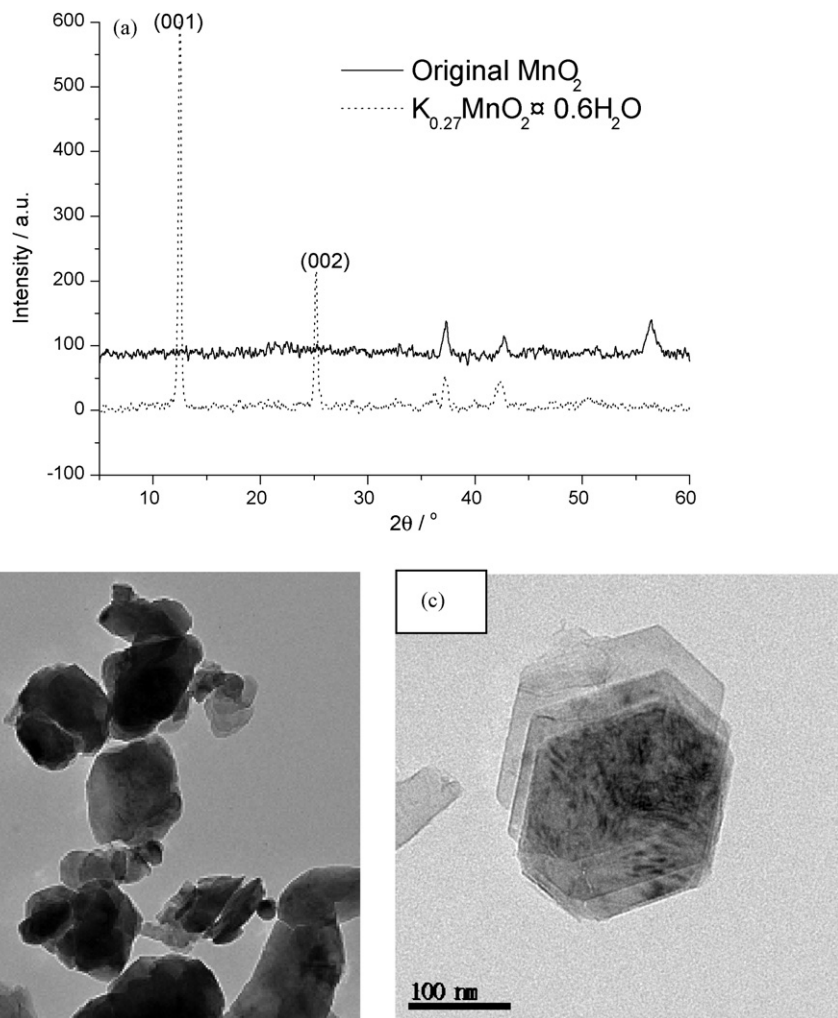


**Fig. 1.** (a) XRD patterns of original  $\text{MnO}_2$  and as-prepared  $\text{K}_{0.27}\text{MnO}_2\text{-}0.6\text{H}_2\text{O}$  powder and TEM images of the as-prepared  $\text{K}_{0.27}\text{MnO}_2\text{-}0.6\text{H}_2\text{O}$ , (b) at low magnification and (c) at high magnification.

layer distance of about 0.7 nm that it could be intercalated by large quaternary ammonium cations and other alkaline cations [18–21].

In the case of an aqueous electrolyte, research has proven that  $\text{K}_2\text{SO}_4$ -based electrolytes show better rate behavior than  $\text{Li}_2\text{SO}_4$ -based electrolyte owing to the smaller hydration ionic radius of  $\text{K}^+$ , weaker solvation interaction between  $\text{K}^+$ -ions and  $\text{H}_2\text{O}$  molecules and higher ionic conductivity of  $\text{K}^+$  than that of  $\text{Li}^+$  [22–25]. In this study, the electrochemical behavior of  $\text{K}_{0.27}\text{MnO}_2\text{-}0.6\text{H}_2\text{O}$  in aqueous  $\text{K}_2\text{SO}_4$  was investigated. Results show that  $\text{K}^+$ -ions can intercalate/deintercalate into/from the  $\text{K}_{0.27}\text{MnO}_2\text{-}0.6\text{H}_2\text{O}$  lattice reversibly during the electrochemical cycles. The assembled asymmetric supercapacitor  $\text{AC}/\text{K}_{0.27}\text{MnO}_2\text{-}0.6\text{H}_2\text{O}$  with 0.5 mol l<sup>-1</sup>  $\text{K}_2\text{SO}_4$  as electrolyte exhibits excellent rate behavior and cycling performance.

## 2. Experimental

$\text{K}_x\text{MnO}_2$  precursor was prepared by ballmilling the mixture of  $\text{K}_2\text{CO}_3$  and  $\text{MnO}_2$  in a molar ratio of 1:2 for 12 h, followed by calcination at 550 °C for 8 h. The precursor was further washed several times with water to remove residual  $\text{K}_2\text{CO}_3$  and dried at 60 °C over night. Elemental analysis by inductively coupled plasma (ICP, Thermo E. IRIS Duo) and thermal gravimetric analysis (TGA, PerkinElmer TGA 7) for the as-prepared powder indicate an approx-

imate composition of  $\text{K}_{0.27}\text{MnO}_2\text{-}0.6\text{H}_2\text{O}$ . The existence of  $\text{H}_2\text{O}$  is caused by the water washing process during the preparation. For comparison, a spinel  $\text{LiMn}_2\text{O}_4$  was also prepared by calcination of the mixtures of  $\text{Li}_2\text{CO}_3$  and  $\text{MnO}_2$  in a stoichiometric ratio at 500 °C for 3 h and then at 700 °C for 8 h. The crystal structures of the samples were characterized by X-ray diffraction (XRD) using a Rigaku D/MAX-IIA X-ray diffractometer with  $\text{Cu K}\alpha$  radiation. Transmission electronic microscopy (TEM) was performed using a JEOL JEM-2010 transmission electron microscope.

For electrochemical tests the cathode was prepared by pressing a mushy mixture of  $\text{K}_{0.27}\text{MnO}_2\text{-}0.6\text{H}_2\text{O}$  (or  $\text{LiMn}_2\text{O}_4$ ), acetylene black and poly(tetrafluoroethylene) (PTFE) (in a weight ratio of 85:10:5) dispersed in ethanol onto Ni-grids. Activated carbon (AC) with a specific surface area of about 2800 m<sup>2</sup> g<sup>-1</sup> measured by BET method was purchased from Ningde Xinseng Chemical and Industrial Co., Ltd. and used as received without further treatment. The AC electrode was prepared in the same way as the cathode. Cyclic voltammetry, galvanostatic charge–discharge tests and electrochemical impedance measurements of the individual electrode were performed using a three-electrode cell, in which a Ni-grid and saturated calomel electrode (SCE) were used as counter and reference electrodes, respectively.

The charge–discharge test of the asymmetric supercapacitor  $\text{AC}/0.5 \text{ mol l}^{-1} \text{K}_2\text{SO}_4/\text{K}_{0.27}\text{MnO}_2\text{-}0.6\text{H}_2\text{O}$  or  $\text{AC}/0.5 \text{ mol l}^{-1} \text{Li}_2\text{SO}_4/\text{LiMn}_2\text{O}_4$  was performed in a two-electrode glass cell sepa-

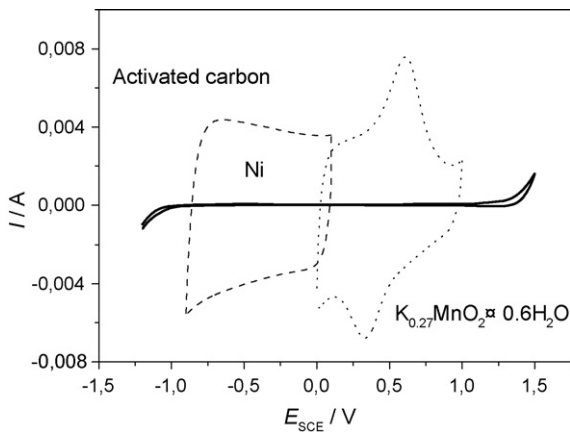


**Fig. 2.** Cyclic voltammograms of activated carbon and  $K_{0.27}MnO_2 \cdot 0.6H_2O$  electrodes in  $0.5 \text{ mol l}^{-1} K_2SO_4$  aqueous solution at a scan rate of  $5 \text{ mV s}^{-1}$ .

rated by non-woven cloth. Electrochemical performance was tested without removal of the oxygen from the solution.

### 3. Results and discussion

XRD patterns of the as-prepared  $K_{0.27}MnO_2 \cdot 0.6H_2O$  and the original material  $MnO_2$  were shown in Fig. 1(a). The original  $MnO_2$  can be indexed as akhtenskite ( $\varepsilon$ - $MnO_2$ , JCPDF No. 89-5171). The final product  $K_{0.27}MnO_2 \cdot 0.6H_2O$  exhibits a lamellar  $\delta$ -type structure with preferred orientation peaks of (001) and (002) [26,27]. A TEM micrograph of the prepared  $K_{0.27}MnO_2 \cdot 0.6H_2O$  at low magnification (Fig. 1(b)) shows aggregated particles with sizes ranging from 50 to 200 nm; the TEM micrograph at high magnification (Fig. 1(c)) shows that these particles exhibit an obviously lamellar structure with thickness of less than 10 nm.

Cyclic voltammograms (CVs) of  $K_{0.27}MnO_2 \cdot 0.6H_2O$  and AC electrodes in  $0.5 \text{ mol l}^{-1} K_2SO_4$  aqueous solution at a scan rate of  $5 \text{ mV s}^{-1}$  are shown in Fig. 2. The current collector, Ni-mesh, is very stable between  $1.0 < E_{SCE} < 1.2 \text{ V}$  in  $K_2SO_4$  aqueous solution owing to the existence of overpotentials [23,25]. The CV of the AC electrode exhibits an ideal rectangular shape without any noticeable redox peak between  $E_{SCE} = 0.1$  and  $-0.8 \text{ V}$ , which is characteristic of a pure electrical double layer capacitance. On the contrary, in the potential range of  $0 < E_{SCE} < 1.0 \text{ V}$ , the  $K_{0.27}MnO_2 \cdot 0.6H_2O$  electrode exhibits a large couple of distinct redox peaks situated at about  $E_{SCE} = 0.35$  and  $0.60 \text{ V}$ , respectively, which can be ascribed to the intercalation/deintercalation of  $K^+$  into/from  $K_{0.27}MnO_2 \cdot 0.6H_2O$  lattice accompanied by the electrochemical conversion between  $Mn^{3+}$  and  $Mn^{4+}$  [21]. Further studies of this intercalation/deintercalation process will be shown later in this report. The large separation between the anodic and cathodic peak can be due to the large kinetic hindrance for the migration of  $K^+$  in the lattice. In addition, this pair of redox peaks is more obviously related to the pseudocapacitance section (typical rectangular section) than that observed for the lamellar  $K_xMnO_2 \cdot H_2O$  prepared from thermal decomposition of  $KMnO_4$  at the same temperature of  $550^\circ\text{C}$  [28]. This may be due to the higher degree of crystallization of the products in our experiments than that in the literature [28]. It can be seen that the XRD patterns of the products synthesized from  $K_2CO_3$  and  $MnO_2$  at  $550^\circ\text{C}$  closely resemble those obtained after thermal decomposition of  $KMnO_4$  at  $800^\circ\text{C}$ . As can be seen from the CV curves of  $K_xMnO_2 \cdot H_2O$  prepared by thermal decomposition of  $KMnO_4$  at various temperatures [28], this pair of redox peaks becomes more obvious with the increase of the degree of crystallization. Moreover, the integrated area of the CV curves of  $K_{0.27}MnO_2 \cdot 0.6H_2O$  during the negative scan is almost equal to that during the positive scan, indicating a reversible Faradic reaction.

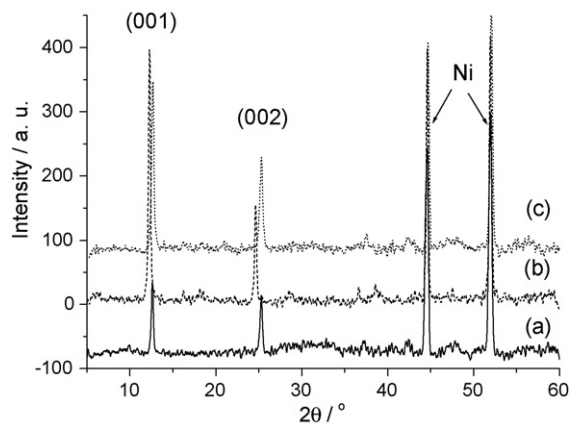


**Fig. 3.** XRD patterns of the  $K_{0.27}MnO_2 \cdot 0.6H_2O$  electrodes (a) prior to cycling, (b) at the end of the first charge and (c) at the end of the following discharge.

In order to further understand the dynamic processes of the  $K_{0.27}MnO_2 \cdot 0.6H_2O$  electrode in  $K_2SO_4$ , *ex situ* XRD patterns of  $K_{0.27}MnO_2 \cdot 0.6H_2O$  electrode prior to cycling, at the end of the first charge ( $1.0 \text{ V}$  vs. SCE) and at the end of the following discharge ( $0 \text{ V}$  vs. SCE) are shown in Fig. 3. After the first charge, the interlayer space shows a slight increase, as can be seen from the shift of the (001) and (002) peaks towards lower values. This may result from the decrease of concentration of  $K^+$ -ions in the interlayer space, which is similar to the behavior of  $LiCoO_2$  upon lithium deintercalation [29]. Elemental analysis by ICP shows that the K/Mn ratio at the end of the first charge is 0.11, much lower than the original value of 0.27, suggesting the deintercalation of  $K^+$  ions. When  $K^+$  ions are extracted from the interlayer space during the charge process, the interlayer separation expands slightly as a result of the weakening of the coordinative interactions between the interlayer  $K^+$ -ions and the oxygen ions in the  $MnO_2$  layers. The extraction of  $K^+$ -ions may be accompanied by the insertion of  $H_2O$  into the interlayer space [21]. At the end of the following discharge, the K/Mn ratio reverts to about 0.27, suggesting the intercalation of  $K^+$ -ions into the interlayer space again. As a result, the interactions between  $K^+$ -ions and oxygen ions increase, and correspondingly the interlayer space decreases slightly, nearly to the original interlayer space prior to cycling. These results suggest the reversible intercalation/deintercalation of  $K^+$  ions in the solid lattice, which are similar to that reported [21].

The potential-time curves of the individual electrode vs. SCE reference electrode and the voltage-time profile of the asymmetric AC// $K_{0.27}MnO_2 \cdot 0.6H_2O$  supercapacitor in  $K_2SO_4$  solution at a current rate of 2 C are shown in Fig. 4. The AC anode presents a typical linear relationship with time, characteristic of electric double layer capacitance. In the case of the  $K_{0.27}MnO_2 \cdot 0.6H_2O$  cathode, the voltage increases slowly during the charge process and exhibits a short plateau at about  $E_{SCE} = 0.6 \text{ V}$ . Correspondingly, the discharge curve decreases slowly and includes a short plateau at  $E_{SCE} = 0.4 \text{ V}$ , suggesting that the Faradic reaction is reversible. This result agrees well with that obtained from CV. The specific capacitance of AC and  $K_{0.27}MnO_2 \cdot 0.6H_2O$  at this current rate is 152.8 and  $144.7 \text{ F g}^{-1}$ , respectively. Therefore, the mass (weight) ratio of AC to  $K_{0.27}MnO_2 \cdot 0.6H_2O$  in the asymmetric supercapacitor is set at 1:1. The asymmetric supercapacitor shows a sloping voltage profile from 0 to  $1.8 \text{ V}$  with excellent reversibility. The specific capacitance and energy density of the AC// $K_{0.27}MnO_2 \cdot 0.6H_2O$  supercapacitor based on the total mass of the active electrode materials (including AC and  $K_{0.27}MnO_2 \cdot 0.6H_2O$ ) at this current rate (about  $50 \text{ W kg}^{-1}$ ) is  $57.7 \text{ F g}^{-1}$  and  $26.0 \text{ Wh kg}^{-1}$ , respectively, which is much higher than those of current symmetric capacitors.

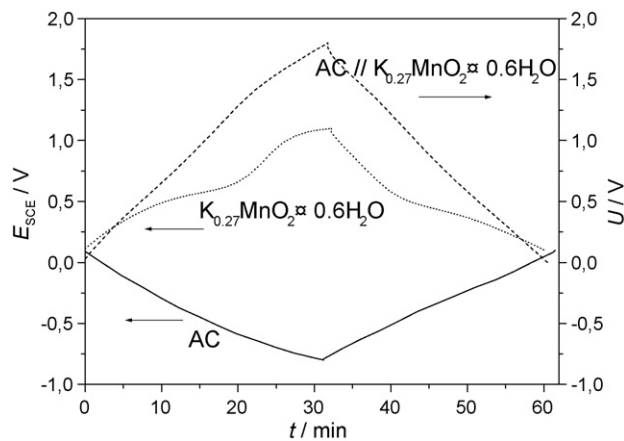


**Fig. 4.** Potential–time curves of the individual electrode vs. SCE reference electrode and the voltage–time profile of the asymmetric  $AC//K_{0.27}MnO_2 \cdot 0.6H_2O$  supercapacitor at a current rate of 2 C in  $0.5\text{ mol l}^{-1} K_2SO_4$  aqueous solution.

The cycling behavior of the asymmetric  $AC//K_{0.27}MnO_2 \cdot 0.6H_2O$  supercapacitor is shown in Fig. 5. It presents excellent cycling behavior, only a slight capacitance loss (<2%) after 10,000 cycles at a current rate of 25 C between 0 and 1.8 V. The coulombic efficiency of the capacitor remains at 100% except in the first several cycles, suggesting that no gas evolution occurred in this voltage range. It is well known that AC shows excellent cycling performance because of its electrical double-layer capacitance. Here,  $K_{0.27}MnO_2 \cdot 0.6H_2O$  with the  $K^+$  ions and  $H_2O$  molecules as pillars also has a very stable lamellar structure during the deintercalation and intercalation of  $K^+$ -ions, which does not transform into other crystalline structures, as can be seen from the XRD patterns of  $K_{0.27}MnO_2 \cdot 0.6H_2O$  electrode before and after 10,000 cycles (Fig. 6). The CV curves of  $K_{0.27}MnO_2 \cdot 0.6H_2O$  electrode during the extended cycles also show no obvious difference (Fig. 7), further suggesting the stability of the lamellar structure of  $K_{0.27}MnO_2 \cdot 0.6H_2O$ .

In addition, it can be seen that the separation between the anodic and cathodic peak during the initial 50 cycles becomes slightly smaller with growing cycle number, suggesting the decrease of the electrode polarization. The electrochemical impedance of  $K_{0.27}MnO_2 \cdot 0.6H_2O$  electrode after 50 cycles also shows a slight decrease compared with that prior to cycling (Fig. 8). The slight decrease of polarization and impedance may be due to an activation process, which favors the electrochemical intercalation/deintercalation of  $K^+$  [23].

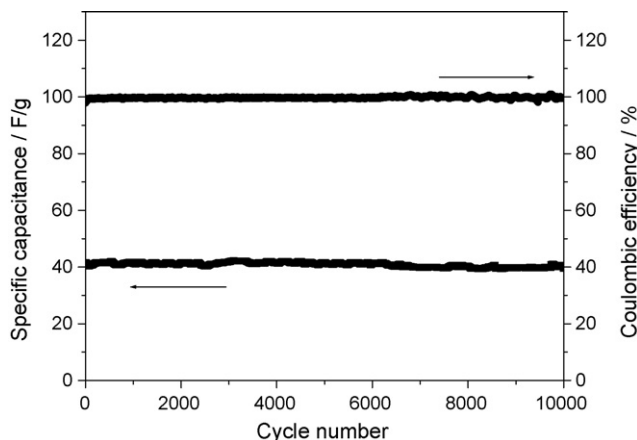


**Fig. 5.** Cycling behavior of the asymmetric  $AC//K_{0.27}MnO_2 \cdot 0.6H_2O$  supercapacitor at a current rate of 25 C between 0 and 1.8 V. The mass (weight) ratio of AC to  $K_{0.27}MnO_2 \cdot 0.6H_2O$  is set at 1:1.

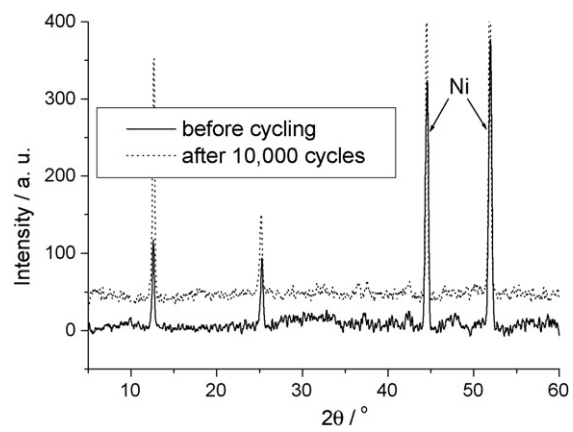


**Fig. 6.** XRD patterns of  $K_{0.27}MnO_2 \cdot 0.6H_2O$  electrode (a) before and (b) after 10,000 cycles.

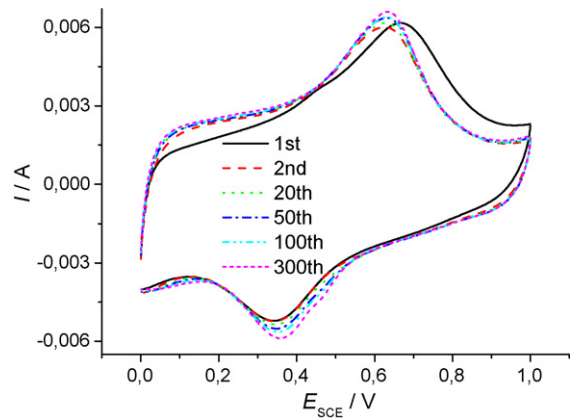


**Fig. 7.** Cyclic voltammograms of  $K_{0.27}MnO_2 \cdot 0.6H_2O$  electrode during the extended cycles at scan rate of  $5\text{ mV s}^{-1}$ .

A Ragone plot of the asymmetric capacitor  $AC//0.5\text{ mol l}^{-1} K_2SO_4//K_{0.27}MnO_2 \cdot 0.6H_2O$  (Fig. 9) shows an energy density  $25.3\text{ Wh kg}^{-1}$  at a power density of  $140\text{ W kg}^{-1}$ , much higher than that of a symmetric  $AC//0.5\text{ mol l}^{-1} K_2SO_4//AC$  capacitor. Moreover, it keeps a very good rate behavior with energy density of  $17.6\text{ Wh kg}^{-1}$  at power density of  $2\text{ kW kg}^{-1}$ , much higher than that of  $AC//0.5\text{ mol l}^{-1} Li_2SO_4//LiMn_2O_4$ . This good rate behavior can be ascribed to the much smaller electrochemical impedance of  $K_{0.27}MnO_2 \cdot 0.6H_2O$  electrode in  $0.5\text{ mol l}^{-1} K_2SO_4$  than that

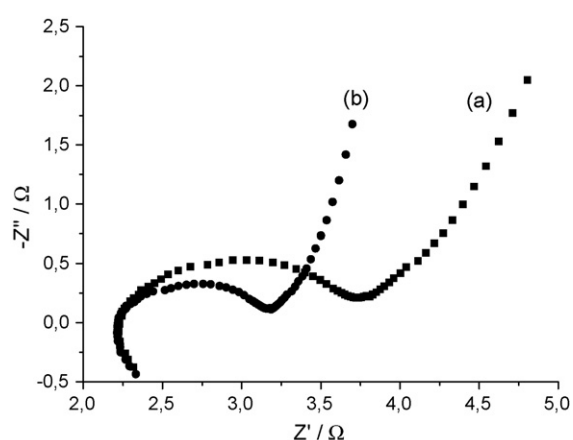


**Fig. 8.** The Nyquist plots of  $K_{0.27}MnO_2 \cdot 0.6H_2O$  electrode (a) before and (b) after 50 cycles.

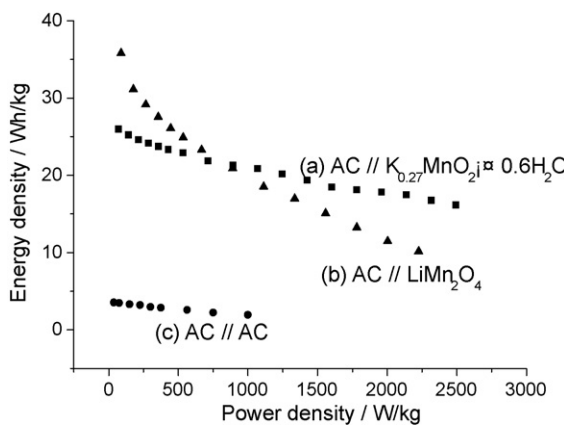


**Fig. 9.** Ragone plots of the asymmetric (a) AC/0.5 mol l<sup>-1</sup> K<sub>2</sub>SO<sub>4</sub>/K<sub>0.27</sub>MnO<sub>2</sub>·0.6H<sub>2</sub>O, (b) AC/0.5 mol l<sup>-1</sup> Li<sub>2</sub>SO<sub>4</sub>/LiMn<sub>2</sub>O<sub>4</sub> and (c) symmetric AC/0.5 mol l<sup>-1</sup> K<sub>2</sub>SO<sub>4</sub>/AC capacitors. The data were calculated based on the total mass of the active electrode materials.

of LiMn<sub>2</sub>O<sub>4</sub> electrode in 0.5 mol l<sup>-1</sup> Li<sub>2</sub>SO<sub>4</sub> (Fig. 10). The small impedance of K<sub>0.27</sub>MnO<sub>2</sub>·0.6H<sub>2</sub>O electrode in K<sub>2</sub>SO<sub>4</sub> may be associated with the lamellar structure of K<sub>0.27</sub>MnO<sub>2</sub>·0.6H<sub>2</sub>O with a large interlayer space for the ionic migration in contrast with the tunnel structure of LiMn<sub>2</sub>O<sub>4</sub>. Moreover, the hydration radius of K<sup>+</sup> (0.331 nm) is smaller than that of Li<sup>+</sup> (0.382 nm), and the ionic conductivity of K<sup>+</sup> (73.5 cm<sup>2</sup> (Ω mol)<sup>-1</sup>) is higher than that of Li<sup>+</sup> (38.6 cm<sup>2</sup> (Ω mol)<sup>-1</sup>) [22–24]. All these factors contribute to the excellent rate behavior of AC/K<sub>2</sub>SO<sub>4</sub>/K<sub>0.27</sub>MnO<sub>2</sub>·0.6H<sub>2</sub>O. In addition, in this asymmetric AC/K<sub>2</sub>SO<sub>4</sub>/K<sub>0.27</sub>MnO<sub>2</sub>·0.6H<sub>2</sub>O capacitor, the supporting electrolyte and the raw material for the preparation K<sub>0.27</sub>MnO<sub>2</sub>·0.6H<sub>2</sub>O are all based on K<sup>+</sup>-salts, which are cheaper and more easily available than Li<sup>+</sup>-salts.

Moreover, in the symmetric AC//AC capacitor, the cations and anions in the electrolyte are depleted during the charge process, thus large amounts of electrolyte are needed to compensate the consumption of electrolyte and ensure sufficient ionic conductivity. However, in the asymmetric AC/K<sub>2</sub>SO<sub>4</sub>/K<sub>0.27</sub>MnO<sub>2</sub>·0.6H<sub>2</sub>O system, K<sup>+</sup> is the working ion and K<sub>0.27</sub>MnO<sub>2</sub>·0.6H<sub>2</sub>O itself could provide K<sup>+</sup> ions, thus the electrolyte concentration is constant during the charge process without electrolyte consumption. Therefore, the weight of electrolyte would be far less than that in the symmetric capacitor. Typically, the electrode material provides about 50% of the total weight of the practical battery, thus the practical specific energy of asymmetric capacitor AC/K<sub>2</sub>SO<sub>4</sub>/K<sub>0.27</sub>MnO<sub>2</sub>·0.6H<sub>2</sub>O

could be up to 13 Wh kg<sup>-1</sup>, which is much higher than that of commercial EDLCs (about 3–5 Wh kg<sup>-1</sup>) and also competitive with that of lead-acid battery (about 15 Wh kg<sup>-1</sup>). Moreover, the asymmetric AC/K<sub>2</sub>SO<sub>4</sub>/K<sub>0.27</sub>MnO<sub>2</sub>·0.6H<sub>2</sub>O capacitor possesses much higher power density, longer cycling life, lower cost, and more environmental friendliness than the current batteries. This asymmetric aqueous AC//K<sub>0.27</sub>MnO<sub>2</sub>·0.6H<sub>2</sub>O capacitor is a promising candidate for the power sources of electric vehicles or other large power devices.

#### 4. Conclusion

Studies of the electrochemical behavior of K<sub>0.27</sub>MnO<sub>2</sub>·0.6H<sub>2</sub>O electrode in K<sub>2</sub>SO<sub>4</sub> solution show the reversible intercalation/deintercalation of K<sup>+</sup> ions in the lattice. An asymmetric supercapacitor with the K<sub>0.27</sub>MnO<sub>2</sub>·0.6H<sub>2</sub>O and AC as cathode and anode, and K<sub>2</sub>SO<sub>4</sub> aqueous solution as electrolyte was successfully assembled. The asymmetric supercapacitor can charge and discharge reversibly in the voltage region of 0–1.8 V without removal of oxygen in the electrolyte and deliver an energy density of 25.3 Wh kg<sup>-1</sup> at power density of 140 W kg<sup>-1</sup> based on the total mass of the active electrode materials. It also shows excellent cycling behavior with no more than 2% capacitance loss after 10,000 cycles at a current rate of 25 C. This asymmetric aqueous AC//K<sub>0.27</sub>MnO<sub>2</sub>·0.6H<sub>2</sub>O capacitor shows promising applications in electric vehicles and other large power devices owing to its low price, good rate behavior and easy preparation of K<sub>0.27</sub>MnO<sub>2</sub>·0.6H<sub>2</sub>O.

#### Acknowledgments

Financial support from National Basic Research Program of China (973 Program No. 2007CB209702), Shanghai Committee of Science and Technology (09QH1400400), Alexander von Humboldt (Institutional Academic Cooperation Program) and Sanyo Chemical Corp. is gratefully acknowledged.

#### References

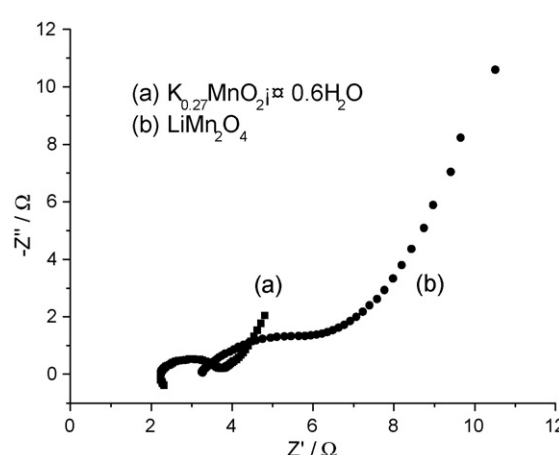


**Fig. 10.** Nyquist plots of (a) K<sub>0.27</sub>MnO<sub>2</sub>·0.6H<sub>2</sub>O and (b) LiMn<sub>2</sub>O<sub>4</sub> electrode at open circuit potential in 0.5 mol l<sup>-1</sup> K<sub>2</sub>SO<sub>4</sub> and Li<sub>2</sub>SO<sub>4</sub>, respectively.

- [1] J.H. Park, O.O. Park, K.H. Shin, C.S. Jin, J.H. Kim, *Electrochim. Solid-State Lett.* 5 (2002) H7–H10.
- [2] A.D. Pasquier, I. Plitz, J. Gural, F. Badway, G.G. Amatucci, *J. Power Sources* 136 (2004) 160–170.
- [3] Y.G. Wang, Y.Y. Xia, *Electrochim. Commun.* 7 (2005) 1138–1142.
- [4] T. Brousse, P.L. Taberna, O. Croisier, R. Dugas, P. Guilletmet, Y. Scudeller, Y. Zhou, F. Favier, D. Bélanger, P. Simon, *J. Power Sources* 173 (2007) 633–641.
- [5] V. Ganesh, S. Pitchumani, V. Lakshminarayanan, *J. Power Sources* 158 (2006) 1523–1532.
- [6] H. Inoue, T. Morimoto, S. Nohara, *Electrochim. Solid-State Lett.* 10 (2007) A261–A263.
- [7] V. Khomenko, E. Raymundo-Piñero, F. Béguin, *J. Power Sources* 177 (2008) 643–651.
- [8] W.H. Jin, G.T. Cao, J.Y. Sun, *J. Power Sources* 175 (2008) 686–691.
- [9] Q. Wang, Z. Wen, J. Li, *Adv. Funct. Mater.* 16 (2006) 2141–2146.
- [10] G.G. Amatucci, F. Badway, A.D. Pasquier, T. Zheng, *J. Electrochem. Soc.* 148 (2001) A930–A939.
- [11] Q.T. Qu, Y. Shi, S. Tian, Y.H. Chen, Y.P. Wu, R. Holze, *J. Power Sources* 194 (2009) 1222.
- [12] Y. Lu, M. Wei, Z. Wang, D.G. Evans, X. Duan, *Electrochim. Acta* 49 (2004) 2361–2367.
- [13] P.K. Sharma, G.J. Moore, F. Zhang, P. Zavalij, M.S. Whittingham, *Electrochim. Solid-State Lett.* 2 (1999) 494–496.
- [14] R. Chen, M.S. Whittingham, *J. Electrochem. Soc.* 144 (1997) L64–L67.
- [15] S.H. Kim, S.J. Kim, S.M. Oh, *Chem. Mater.* 11 (1999) 557–563.
- [16] Y. Lu, L. Yang, M. Wei, Y. Xie, T. Liu, *J. Solid State Electrochem.* 11 (2007) 1157–1162.
- [17] J. Ge, L. Zhuo, F. Yang, B. Tang, L. Wu, C. Tung, *J. Phys. Chem. B* 110 (2006) 17854–17859.
- [18] Y. Omomo, T. Sasaki, L. Wang, M. Watanabe, *J. Am. Chem. Soc.* 125 (2003) 3568–3575.
- [19] L. Wang, Y. Omomo, N. Sakai, K. Fukuda, I. Nakai, Y. Ebina, K. Takada, M. Watanabe, T. Sasaki, *Chem. Mater.* 15 (2003) 2873–2878.
- [20] M. Nakayama, S. Konishi, H. Tagashira, K. Ogura, *Langmuir* 21 (2005) 354–359.
- [21] H. Kanoh, W. Tang, Y. Makita, K. Ooi, *Langmuir* 13 (1997) 6845–6849.

- [22] R.N. Reddy, R.G. Reddy, *J. Power Sources* 124 (2003) 330–337.
- [23] Q.T. Qu, B. Wang, L.C. Yang, Y. Shi, S. Tian, Y.P. Wu, *Electrochem. Commun.* 10 (2008) 1652–1655.
- [24] A.C. Partridge, C. Milestone, C.O. Too, G.G. Wallace, *J. Memb. Sci.* 132 (1997) 245–253.
- [25] Q.T. Qu, P. Zhang, B. Wang, Y.H. Chen, S. Tian, Y.P. Wu, R. Holze, *J. Phys. Chem. C* 113 (2009) 14020.
- [26] Y. Kadoma, Y. Uchimoto, M. Wakihara, *J. Phys. Chem. B* 110 (2006) 174–177.
- [27] S. Komaba, N. Kumagai, S. Chiba, *Electrochim. Acta* 46 (2000) 31–37.
- [28] H.Y. Lee, V. Mnivannan, J.B. Goodenough, C.R. Acad. Sci. Série II c: Chim. (1999) 565–577.
- [29] Y.P. Wu, X.B. Dai, J.Q. Ma, Y.J. Cheng, *Lithium Ion Batteries—Practice and Applications*, Chemical Industry Press, 2004.